The Effect of Diamondlike Carbon Overcoat on the Tribological Performance of the Dimple/Gimbal Interface in Hard Disk Drives[1]

Youyi Fu[2]
Center for Memory and Recording Research,
University of California, San Diego,
9500 Gilman Drive,
La Jolla, CA 92093-0401
e-mail: yof001@ucsd.edu

Vlado A. Lubarda
Department of NanoEngineering,
University of California, San Diego,
9500 Gilman Drive,
La Jolla, CA 92093-0448
e-mail: vlubarda@ucsd.edu

Frank E. Talke
Fellow ASME
Center for Memory and Recording Research,
University of California, San Diego,
9500 Gilman Drive,
La Jolla, CA 92093-0401
e-mail: ftalke@ucsd.edu

Fretting wear at the dimple/gimbal interface of a hard disk drive suspension was investigated for stainless steel dimples in contact with stainless steel gimbals coated with diamondlike carbon (DLC) of different thicknesses and different elastic moduli. Scanning electron microscopy (SEM) was used to evaluate the size and characteristics of the wear scar of both the dimple and the gimbal. Fretting wear and fatigue-type cracks were found predominantly on the dimple. For different dimple/gimbal combinations tested in this study, the least amount of wear was obtained for the case of a 690 nm thick DLC overcoat. Numerical simulations were performed to calculate the maximum principal stress in the dimple and the gimbal with the goal of correlating wear and the maximum principal stress. The maximum principal stress in both the dimple and the gimbal was found to increase with an increase of the elastic modulus of the DLC overcoat on the gimbal. On comparing the experimental and simulation results, we conclude that wear and fatigue crack formation can be explained by the different level of the maximum principal stress in both the dimple and the gimbal. [DOI: 10.1115/1.4032797]

Keywords: contact mechanics, crack, diamondlike carbon, dimple/gimbal interface, elasticity, fatigue, fretting wear, hard disk drive, overcoat, principal stress

1 Introduction

Fretting wear is defined as damage of tribosurfaces caused by small-amplitude oscillatory relative displacements [1]. A typical example of fretting wear occurs in the dimple/gimbal interface of a hard disk drive suspension. As shown in Figs. 1(*a*) and 1(*b*), a spherical protrusion on the suspension, called the "dimple," is in contact with a flat part of the flexure spring, the so-called "gimbal." The contact point between the dimple and the gimbal allows roll and pitch motion of the slider in response to the applied external forces. The roll and pitch motion of the slider during track seeking and track following causes small-amplitude oscillatory relative displacements between the dimple and the gimbal, leading to fretting wear and the formation of wear particles. The presence of wear particles in a hard disk drive is undesirable because it can lead to failure of the head disk interface.

In the last decade, several studies of fretting wear at the dimple/gimbal interface of a hard disk drive suspension have been performed. Raeymaekers et al. [2] investigated the relationship between normal load and wear particle generation. In addition, they studied the effect of surface roughness of the gimbal on the tribological performance of the dimple/gimbal interface. In another study, Raeymaekers et al. [3] studied the tribological degradation of nickel-coated and gold-coated gimbals against stainless steel dimples and observed a substantial reduction in friction and wear with an increase of the overcoat thickness. Yoon et al. [4] observed a similar result for wear of a stainless steel dimple in contact with a gold-coated gimbal. Li et al. [5] analyzed the change of the plasticity index of nonpolished and laser-polished dimples during fretting wear. In a related study, Li et al. [6] created a finite element model of the interface and showed that high normal load is advantageous for reducing relative motion between the dimple and the gimbal, and for reducing fretting wear at the dimple/gimbal interface.

Although investigations in Refs. [2–6] have shown in detail the mechanism of wear at the dimple/gimbal interface, none of the above studies has dealt with the effect of a DLC overcoat on fretting wear. It is well known that a DLC overcoat has a low friction coefficient and can reduce wear at contact surfaces dramatically [7–9]. Consequently, in this study, fretting wear of a stainless steel dimple was investigated in contact with a stainless steel gimbal coated with a thin layer of DLC. The coefficient of friction was measured using a load cell, and the wear scar was evaluated using SEM. The present study is an extension of the experimental work reported in Refs. [3–5] on fretting wear at the dimple/gimbal interface for the case of a thin carbon overcoat, although the nickel-coated and the gold-coated gimbals in Refs. [3,4] were tested at different experimental conditions (number of cycles, frequency, and normal load). Both experimental and numerical studies were performed to investigate the effect of the thickness and the elastic modulus of the DLC overcoat on the tribological performance of the dimple/gimbal interface in hard disk drives.

2 Materials and Methods

*F*retting wear generated at the dimple/gimbal interface is caused by pitch and roll motion of the slider. In our work, we modeled the motion between the dimple and the gimbal along a fixed direction, so that the measured friction coefficient corresponds to this relative motion and the corresponding changes of the contact surfaces. As shown in Fig. 2, a hard disk drive suspension was attached to the suspension mount using a single screw. The vertical position of the suspension was adjusted using a dial

[1]This paper is designated as a tribute to Fred Ling.
[2]Corresponding author.
Contributed by the Tribology Division of ASME for publication in the JOURNAL OF TRIBOLOGY. Manuscript received June 15, 2015; final manuscript received August 25, 2015; published online July 8, 2016. Assoc. Editor: Min Zou.

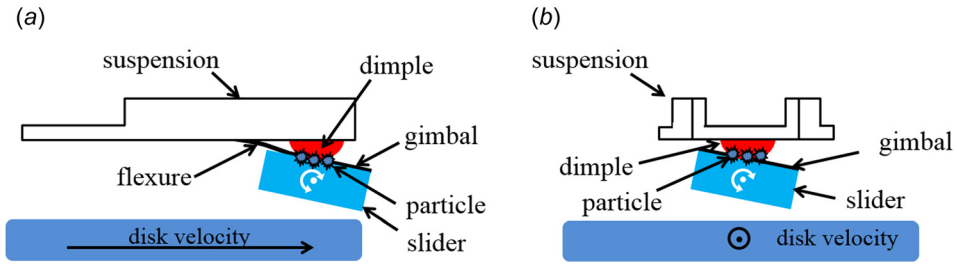

Fig. 1 Schematic of the head/disk interface: (*a*) pitch motion and (*b*) roll motion of slider

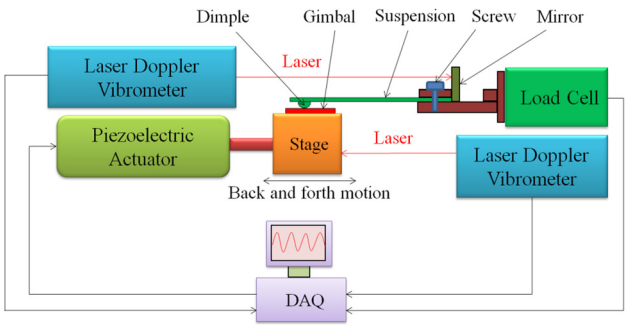

Fig. 2 Schematic of the fretting wear tester

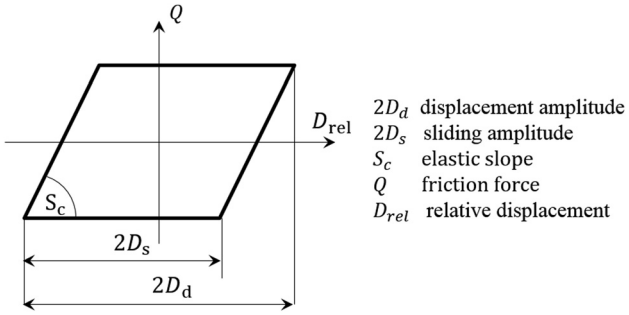

Fig. 3 Typical friction hysteresis loop

gauge to apply a normal load of 20 mN, in agreement with the typical preload of the dimple/gimbal interface in a hard disk drive. The gimbal was mounted on a stage attached to a piezoelectric actuator. A triangular voltage input signal was applied to the piezoelectric actuator, resulting in horizontal movement of the gimbal relative to the dimple. The displacement amplitude $2D_d$ was approximately 10 μm. A load cell attached to the suspension mounting block was used to measure the friction force, while two independent laser Doppler vibrometers (LDVs) were used to measure the horizontal displacement of the gimbal and the suspension. The difference between the two LDV measurements gives the relative displacement between the dimple and the gimbal. For each dimple/gimbal interface, a fretting wear test was performed with a total number of 3.45×10^6 cycles at a frequency of 20 Hz. The duration for each test was 48 hrs. The data were collected in real time using a data-acquisition board and LABVIEW, a commercially available software.

An idealized friction versus displacement curve, also known as the "friction hysteresis loop" [4], is shown in Fig. 3. The dissipated energy E_μ for each cycle is determined by numerical integration of the area enclosed by this loop. The average coefficient of friction μ can be calculated from the dissipated energy E_μ, the displacement amplitude $2D_d$, and the normal load N according to Ref. [10]

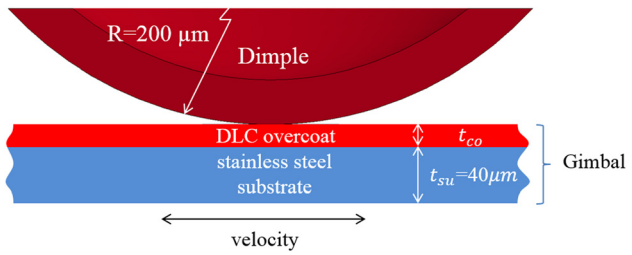

Fig. 4 Schematic of the dimple/gimbal interface coated with a thin layer of DLC. The radius of the spherical dimple is 200 μm. The thickness of the stainless steel substrate of the gimbal t_{su} is 40 μm. The thickness of the DLC overcoat t_{co} is 15 nm, 70 nm, 250 nm, and 690 nm, respectively.

$$\mu = \frac{E_\mu}{4 \cdot D_d \cdot N} \tag{1}$$

A schematic of the dimple/gimbal interface is shown in Fig. 4. Five different dimple/gimbal combinations were used (Table 1). Dimples were made from stainless steel (304 SST). The dimples are spherical protuberances with a radius of 200 μm. DLC overcoats, ranging in thickness from 15 nm to 690 nm, were deposited on stainless steel substrate (304 SST) of 40 μm thickness. The carbon overcoat was produced using filtered cathodic vacuum arc. The 15 nm DLC overcoat consists of tetrahedral amorphous carbon (ta-C). The other three DLC overcoats are hydrogenated tetrahedral amorphous carbon (ta-C:H). The average surface roughness of the four DLC-coated gimbals is close to 200 nm. Uncoated gimbals were used as control group for this study.

3 Experimental Results and Discussion

3.1 Coefficient of Friction. Figure 5 shows the coefficient of friction as a function of the number of fretting wear cycles for different dimple/gimbal material combinations. Each curve is the average of three tests obtained for the same conditions. As seen in Fig. 5, the friction coefficient for all the material combinations increases slightly with the number of fretting wear cycles. The lowest friction coefficient was found for a carbon overcoat thickness of 690 nm (Fig. 5(*d*)), while the highest coefficient of friction occurred for a carbon overcoat thickness of 250 nm (Fig. 5(*c*)). The coefficient of friction for the 690 nm DLC overcoat showed fewer fluctuations than any of the other material combinations, most likely related to the fact that fewer wear particles were generated in the case of the 690 nm thick DLC overcoat. The mean friction coefficient for 3.45×10^6 fretting wear cycles is shown in Fig. 6. We observe that the mean friction coefficient for the 15 nm DLC overcoat is about 0.28. The friction coefficient increases to 0.41 for the 250 nm DLC overcoat and decreases to approximately 0.25 for an overcoat thickness of 690 nm. The mean friction coefficient for an uncoated gimbal is 0.33. The increase of the friction coefficient with the number of cycles is most likely related to the change of the surface roughness and the generation of wear particles during the test. The smaller friction

Table 1 Dimple/gimbal materials combination tested

	A	B	C	D	E
Dimple	304 stainless steel	304 stainless steel	304 stainless steel	304 stainless steel	304 stainless steel
Gimbal	304 stainless steel coated with 15 nm DLC (ta-C)	304 stainless steel coated with 70 nm DLC (ta-C:H)	304 stainless steel coated with 250 nm DLC (ta-C:H)	304 stainless steel coated with 690 nm DLC (ta-C:H)	304 stainless steel without DLC

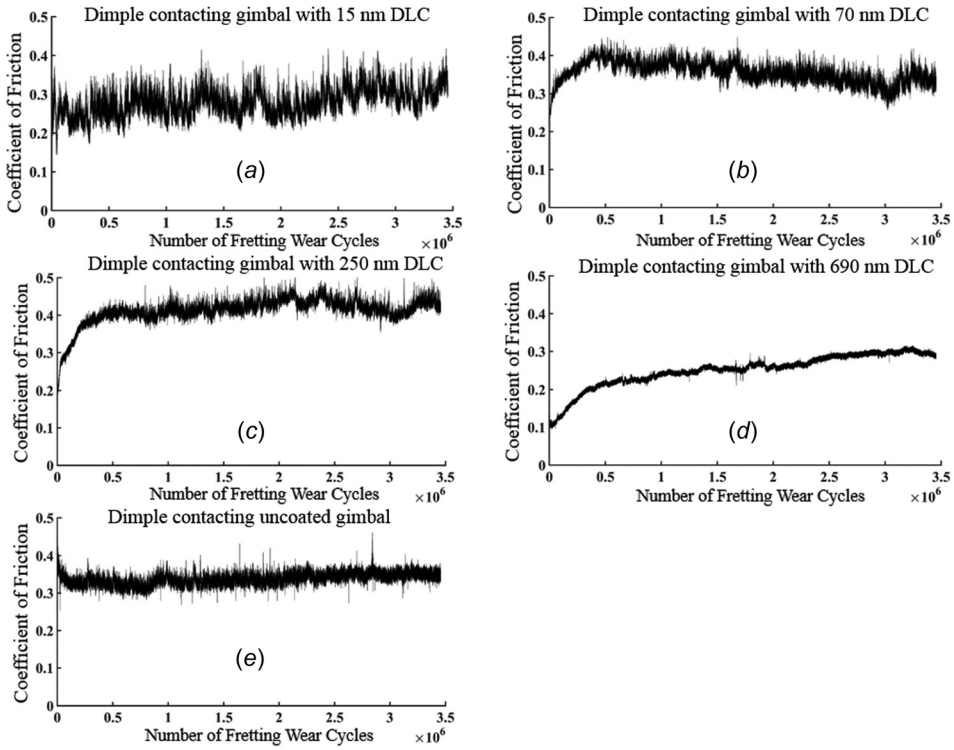

Fig. 5 Coefficient of friction versus number of fretting wear cycles for (*a*) 15 nm DLC-coated gimbal, (*b*) 70 nm DLC-coated gimbal, (*c*) 250 nm DLC-coated gimbal, (*d*) 690 nm DLC-coated gimbal, and (*e*) uncoated gimbal

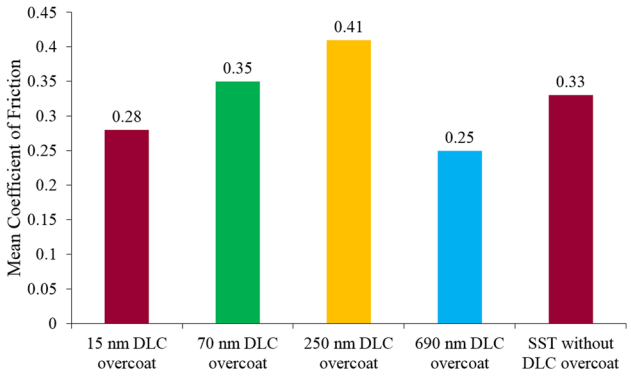

Fig. 6 Mean coefficient of friction for different dimple/gimbal combinations

coefficient observed for the 690 nm DLC overcoat appears to be related to the formation of a transfer layer [11] on the gimbal. This point will be further discussed later in the paper.

3.2 Wear Scar on Dimple. Figure 7 shows the SEM images of wear scars on stainless steel dimples after 3.45×10^6 fretting wear cycles against gimbals coated with a DLC overcoat of 15 nm, 70 nm, 250 nm, and 690 nm thickness and a gimbal without a DLC overcoat. The top row in Fig. 7 corresponds to 1500× magnification, while the bottom row is for 6000× magnification. We observe that the wear scar on the dimple in Fig. 7(*d*) is much smaller than the wear scar on the other dimples (Figs. 7(*a*)–7(*c*) and 7(*e*)). Comparing the wear scar in Fig. 7(*d*) with the wear scar in Figs. 7(*a*)–7(*c*) and 7(*e*), we observe that fewer wear particles are present in Fig. 7(*d*) than in Figs. 7(*a*)–7(*c*) or 7(*e*). In addition, the size of the wear particles in Fig. 7(*d*) is smaller than the size of the wear particles in the other cases. Energy dispersive X-ray (EDX) analysis shows that these wear particles have the same chemical composition as the dimple, suggesting that the wear particles come from the dimple. In addition, we observe that the wear scar in Fig. 7(*d*) does not show any distinct black regions as can be seen on other samples. From EDX analysis, we observe that the percentage of oxygen in the black regions of the dimple increased from 6% to 25% after the fretting wear test, which implies that the dimple material is oxidized during the fretting wear test. The absence of dark regions in Fig. 7(*d*) suggests that the wear scar has not oxidized. From the SEM images at 6000× magnification shown in Fig. 7, we observe the appearance of microcracks in Figs. 7(*a*)–7(*c*) and 7(*e*). Microcracks were absent on dimples tested against gimbals with a 690 nm DLC overcoat (Fig. 7(*d*)).

3.3 Wear Scar on Gimbal. Figure 8 shows the SEM images of wear scars of different gimbals after 3.45×10^6 fretting wear

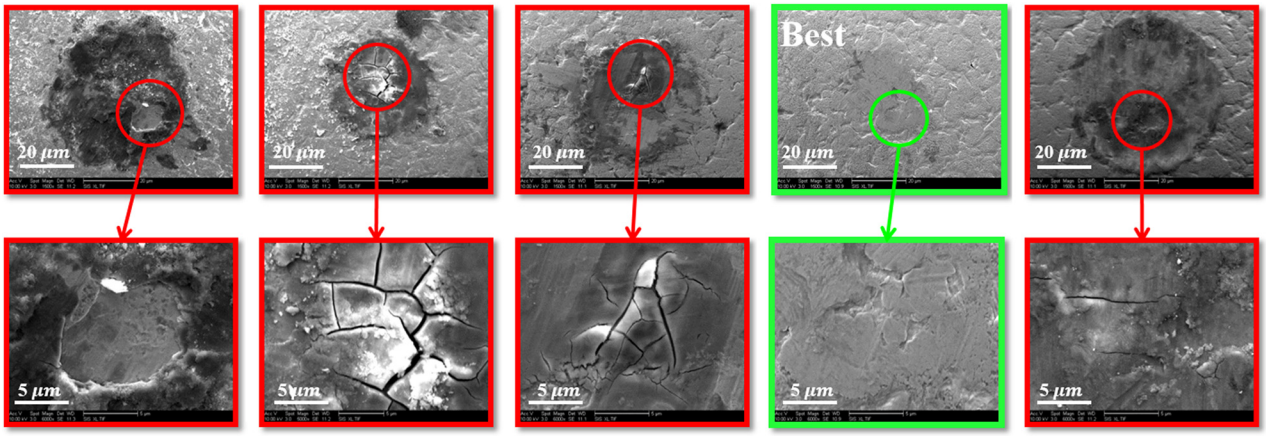

Fig. 7 SEM images of the typical wear scars on stainless steel dimples after 3.45×10^6 fretting wear cycles against (*a*) 15 nm DLC-coated gimbal, (*b*) 70 nm DLC-coated gimbal, (*c*) 250 nm DLC-coated gimbal, (*d*) 690 nm DLC-coated gimbal, and (*e*) uncoated gimbal

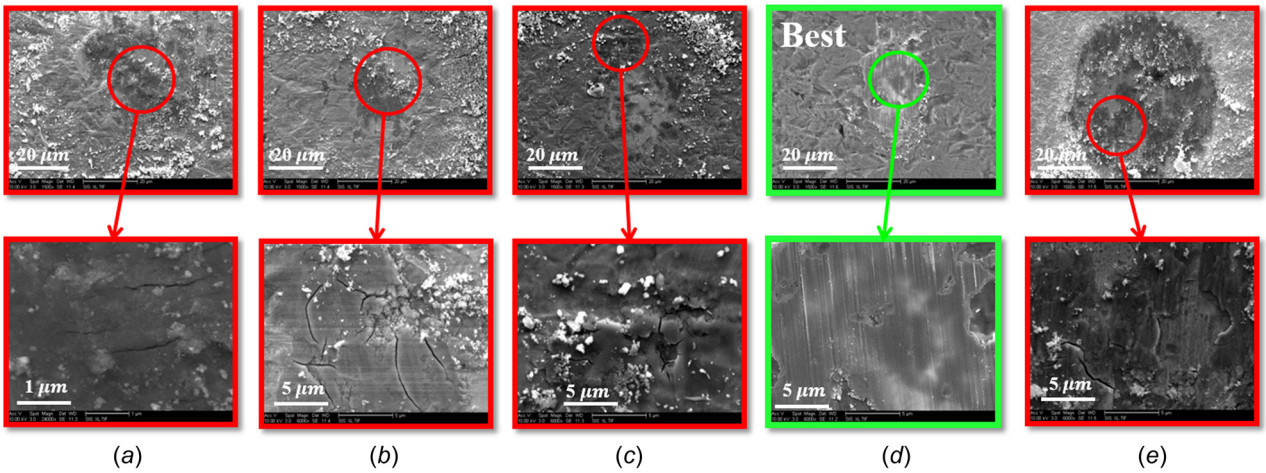

Fig. 8 SEM images of the typical gimbal wear scars on (*a*) 15 nm DLC-coated gimbal, (*b*) 70 nm DLC-coated gimbal, (*c*) 250 nm DLC-coated gimbal, (*d*) 690 nm DLC-coated gimbal, and (*e*) uncoated gimbal, after 3.45×10^6 fretting wear cycles

cycles. The high-magnification SEM images in Fig. 8 show the region at the center of the gimbal wear scars. We observe the presence of microcracks *in the wear scars of gimbal A, B, C, and E* (Figs. 8(*a*)–8(*c*) and 8(*e*)), but none in the wear scar of gimbal D (Fig. 8(*d*)). The uncoated gimbal has the largest cracks (Fig. 8(*e*)). The gimbal coated with 15 nm DLC (Fig. 8(*a*)) showed the smallest cracks. Gimbals coated with 70 nm DLC (Fig. 8(*b*)) and 250 nm DLC (Fig. 8(*c*)) showed cracks of similar size. From Fig. 8(*d*), we observe that a thin layer has formed in the contact area of the gimbal with a 690 nm thick DLC overcoat. This thin layer is likely to be a transfer layer [11]. EDX analysis was performed on the transfer layer. The results showed that the transfer layer is primarily carbon, which suggests that it is generated from the DLC overcoat. As reported in Ref. [11], a transfer layer can be formed by the graphitization of the DLC overcoat and the distortion of the DLC structure. Among the four DLC overcoats tested in this study, the 690 nm thick DLC layer has the lowest sp^3 bonding ratio of 67% as measured by electron energy loss spectroscopy (EELS). Thus, it is most likely that the 690 nm thick DLC layer is graphitized. The transfer layer formed on the 690 nm thick DLC overcoat can act as a solid lubricant and reduce the friction coefficient at the contact interface [12]. Therefore, the formation of the transfer layer could explain why the coefficient of friction of the 690 nm DLC-coated gimbal was low and why the surface damage was less than that observed on other gimbals (Figs. 8(*a*)–8(*c*) and 8(*e*)). Based on the absence of cracks and the reduced number of wear particles in Figs. 7(*d*) and 8(*d*), we conclude that gimbals coated with a 690 nm DLC film have the best protection against fretting wear.

We infer from Figs. 7(*e*) and 8(*e*) that the contact areas of both the stainless steel dimple and the stainless steel gimbal are oxidized during the fretting wear test. For other cases in which the gimbal is coated with DLC, only the contact area of the dimple is oxidized. Thus, the DLC overcoat prevents the gimbal from being oxidized, which may explain why the DLC overcoat improves the tribological performance of the dimple/gimbal interface.

3.4 Wear Mechanism. As observed from Fig. 7, shallow fatigue-type surface cracks of different lengths are present on the dimple surface after a fretting wear test. The formation of these cracks is related to the change of stress from tensile to compressive during each fretting cycle and appears to be a function of the mechanical properties, the thickness of the DLC overcoat, the bonding strength between the DLC overcoat and the substrate, and the number of fretting wear cycles. To understand the formation of cracks and the wear characteristics of the dimple/gimbal interface, we focus in the remainder of this paper on the effect of

mechanical properties of the dimple and the gimbal and the effect of the thickness of the DLC overcoat.

The first step in the understanding of crack formation and wear is to determine the mechanical properties of the carbon overcoat such as its elastic modulus and hardness. In general, nanoindentation techniques are used to determine such properties of thin coatings [13]. However, in the case of a very thin overcoat on the order of 10 nm, nanoindentation measurements are strongly influenced by the underlying substrate [14]. To avoid this effect, it is common to characterize a very thin carbon overcoat using EELS [15]. In EELS measurement, the sp^3 bonding fraction of the carbon overcoat is determined. According to Xu et al. [16], the elastic modulus E and the indentation hardness H of a DLC overcoat are nearly proportional to the sp^3 fraction of the DLC overcoat. Therefore, we assume that the elastic modulus E and the indentation hardness H of a DLC overcoat can be calculated using the expressions

$$E = ar - b \tag{2}$$

$$H = cr - d \tag{3}$$

where r is the sp^3 fraction of the DLC overcoat obtained from EELS measurement. The coefficients a (1600 GPa), b (1010 GPa), c (256 GPa), and d (173 GPa) are values obtained by performing a linear fit for the data reported by Xu et al. [16]. Figure 9 shows the sp^3 fractions, the elastic modulus, and the hardness of the four DLC overcoats used in this study. As shown in Fig. 9(*a*), the sp^3 fraction of the 15 nm, 70 nm, 250 nm, and 690 nm DLC overcoats is 90%, 70%, 70%, and 67%, respectively. Using the sp^3 measurement, we obtain values for the elastic modulus of the 15 nm, 70 nm, 250 nm, and 690 nm DLC overcoats to be 430 GPa, 110 GPa, 110 GPa, and 62 GPa, respectively, as shown in Fig. 9(*b*). The elastic modulus of the 690 nm DLC overcoat (62 GPa) is close to 70 GPa as measured using nanoindentation. As shown in Fig. 9(*c*), the hardness of the 15 nm, 70 nm, and 250 nm DLC overcoats is 57.4 GPa, 6.2 GPa, and 6.2 GPa, respectively, obtained by applying Eq. (3). Nanoindentation shows that the hardness of the 690 nm DLC overcoat is 6.0 GPa. The dotted lines in Figs. 9(*b*) and 9(*c*) indicate the elastic modulus (200 GPa) and the hardness (5.0 GPa) of the stainless steel dimple.

Xie and Williams [17] and others [18,19] have shown that for a soft surface sliding against a hard surface, wear occurs mainly on the softer surface. As shown in Fig. 9(*c*), for case A (15 nm DLC overcoat), the hardness of the dimple material (5.0 GPa) is much smaller than that of the hardness of the DLC overcoat (57.4 GPa). Therefore, wear and material removal should be observed predominately on the softer dimple surface (Fig. 7(*a*)). Since the DLC overcoat on the gimbal is harder than the dimple material, wear and crack formation on the gimbal (Fig. 8(*a*)) is expected to be less pronounced than on the dimple (Fig. 7(*a*)). For cases B and C, the hardness of the DLC overcoat is close to the hardness of the dimple. During the fretting wear test, the same region of the dimple keeps contacting the gimbal throughout the test, while the contact region of the gimbal changes with the back and forth motion of the gimbal. Therefore, large cracks are present on the dimple material (Figs. 7(*b*) and 7(*c*)) but smaller cracks are observed on the gimbal material (Figs. 8(*b*) and 8(*c*)). For case D (690 nm DLC overcoat), we did not observe any cracks on either the dimple (Fig. 7(*d*)) or the gimbal surface (Fig. 8(*d*)). This result is most likely a consequence of the formation of the transfer layer.

Comparing the gimbal coated with DLC (Figs. 8(*a*)–8(*d*)) and the uncoated gimbal (Fig. 8(*e*)), we observe that cracks on the gimbals coated with DLC (Figs. 8(*a*)–8(*d*)) are smaller than cracks formed on the uncoated gimbal (Fig. 8(*e*)). This suggests that the tribological performance of the gimbal is improved by the DLC overcoat. However, the increased elastic modulus of the DLC overcoat causes higher contact stresses, leading to an increase in the wear of the dimple. Furthermore, only small cracks on the order of 1 μm were observed on the gimbal coated with 15 nm DLC (Fig. 8(*a*)), while large cracks on the order of 10 μm were formed on the mating dimple (Fig. 7(*a*)).

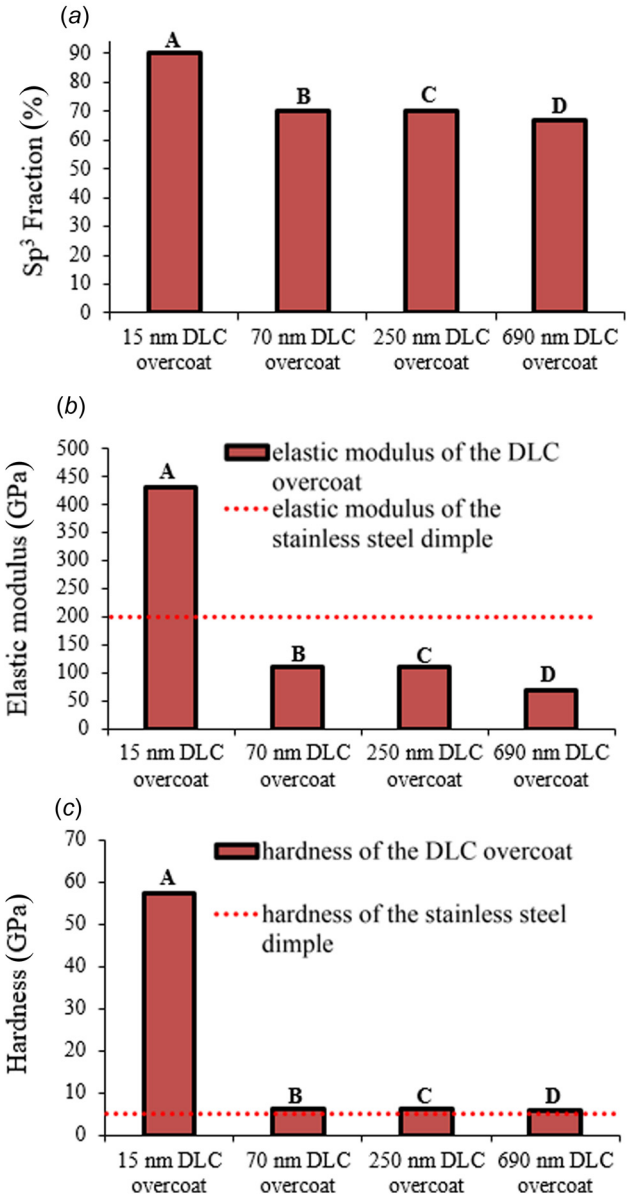

Fig. 9 (*a*) sp^3 fraction, (*b*) elastic modulus, and (*c*) hardness of 15 nm, 70 nm, 250 nm, and 690 nm DLC overcoats

4 Numerical Simulation Results and Discussion

4.1 Finite Element Model. From the fretting wear test results, we have observed that DLC overcoats on a gimbal affect the number of wear particles and the formation of fatigue cracks on the dimple and the gimbal. To understand the effect of material properties and the thickness of the DLC overcoat on the wear characteristics and crack formation at the dimple/gimbal interface, we turn next to the calculation of the contact stress between the dimple and the gimbal. Since the generation of wear particles and the formation of fatigue cracks are related to the maximum principal tensile stress [20], we will use principal stress as metric for analyzing the simulation results.

The contact between the dimple and the gimbal is a contact problem of a hemisphere sliding back and forth against a flat surface coated with a thin layer of material as shown in Fig. 4. In addition to the normal load, a frictional force with alternating sign is present at the interface in a fretting wear situation. To calculate the contact stress, a model involving both the normal and tangential force is needed. The classical Hertzian contact model [21] is not applicable since it includes only a normal load. The reciprocal

motion between the dimple and the gimbal causes friction at the contact interface, and the direction of the friction force changes with each cycle. Hamilton [22] developed a set of equations for calculating the contact stresses between two bodies in the presence of normal and tangential load. However, his model applies only to the case of homogeneous materials, which is not the case for the gimbal coated with a thin DLC overcoat as shown in Fig. 4. Ling et al. [23] studied the problem of a layered elastic half-space under a moving load, but in their model the friction force was not included. O'Sullivan and King [24] used Papkovich–-Neuber elastic potentials to calculate the contact stress for sliding contact between a spherical indenter and a layered half-space. In their method, a numerical inverse Fourier transform and a least squares fitting approach are used to obtain the contact pressure. Since no easy-to-use closed-form equations exist for the case of a hemisphere sliding on a half-space coated with a thin layer, finite-element analysis was used to calculate the contact stress between the dimple and a gimbal coated with a thin DLC overcoat.

Figure 10(*a*) shows a three-dimensional finite element model for a dimple sliding against a stainless steel gimbal coated with a thin DLC overcoat. The blow-up of the contact region is shown in Fig. 10(*b*). In the calculations, the DLC overcoat thickness t_{co} was chosen to be 15 nm, 70 nm, 250 nm, and 690 nm, respectively. These values are the same as the thickness of the DLC overcoat used in our fretting wear tests. The thickness of the stainless steel substrate of the gimbal t_{su} is 40 μm. The radius of the stainless steel dimple R is 200 μm. A combination of eight-node brick elements and six nodes pentahedron elements was used to model the dimple. The gimbal substrate and the DLC overcoat were modeled using eight-node brick elements. Because the tangential motion of the gimbal is in the horizontal direction (x direction), the model is symmetric with respect to the x–z plane. Thus, only half of the dimple and the gimbal are modeled. Nodes at the top of the dimple are fixed in all six degrees-of-freedom. Nodes on the x–z plane are restrained from motion in the y direction. A displacement of 10 μm along the x direction is applied to the gimbal. Both the normal and the tangential load are considered. A distributed normal load N/n is applied to each node at the bottom of the gimbal in the positive z direction, with the number of nodes n on the bottom of the gimbal being equal to 416. The normal load N is 10 mN, corresponding to half the normal load applied in the fretting wear test since our model simulates only half of the dimple and half of the gimbal. In the finite element model, the tangential force Q is the friction force between the dimple and the gimbal, given by

$$Q = \mu \cdot N \tag{4}$$

where μ is the friction coefficient between the dimple and the gimbal. The dimple and gimbal materials are assumed to be elastic. The elastic modulus of the DLC overcoat and the friction coefficient used in the simulation were obtained from EELS measurements and fretting wear tests, respectively. The numerical calculations were performed using the explicit solver of the commercially available finite-element analysis software LS-DYNA [25].

4.2 Stress Distribution in the Dimple. Figure 11 shows the distribution of the maximum principal stress around the contact area of the dimple, for the gimbal coated with 690 nm DLC, sliding in the positive x direction (Fig. 11(*a*)) and the negative x direction (Fig. 11(*b*)). Since reciprocating sliding contact between the dimple and the gimbal is a quasi-static contact problem [26], the stress distribution in the dimple and the gimbal does not change with time over the contact region, assuming the friction remains constant throughout a fretting wear cycle. Thus, the stress distributions shown in this paper correspond to arbitrary sliding positions between 0 and 10 μm. We observe from Fig. 11 that the largest maximum principal tensile stress of about 80 MPa occurs in the dimple at the trailing edge of the contact zone. If the sliding direction of the gimbal is reversed, the location of the largest maximum principal tensile stress changes to the leading edge of the contact zone. At this position, the maximum principal tensile stress varies for each pass between 0 and 80 MPa as the gimbal moves back and forth. Microcracks generated by this type of cyclic stresses are called "fretting fatigue cracks" [27].

Cracks due to fretting fatigue are likely to start at pre-existing material flaws, such as inclusions and voids, or they are created as the result of dislocation movements [28]. Since the typical fatigue crack length on the dimples in our experiments is on the order of 10–20 μm, we refer to these cracks as "short fatigue cracks" [29]. In fracture mechanics, the stress intensity factor is commonly used to characterize the stress field ahead of a crack tip [30]. It was shown in Ref. [31] that a short fatigue crack can propagate even if the stress intensity factor at the tip of the crack is far below the threshold value of the stress intensity factor for long fatigue cracks. Although the propagation criteria developed by Paris and Erdogan [32] for long fatigue cracks may not strictly apply in our case, it is useful to calculate the range of cyclic stress $\Delta\sigma$ and then use this value in trying to explain the different crack patterns observed in the experiments, under the assumption that the propagation of short fatigue crack is proportional to $\Delta\sigma$ [33]. Since the smallest maximum principal tensile stress at the edge of the contact area of the dimple is zero during each cycle, the range of cyclic stress $\Delta\sigma$ at the edge of the contact area of the dimple is equal to the largest maximum principal tensile stress σ_{max}. We will use this value to interpret our simulation results.

Figure 12 shows the distribution of the maximum principal stress around the contact area of a dimple as the carbon-coated gimbal moves in the positive x direction. Simulation results are shown for a dimple contacting a gimbal with a DLC overcoat thickness of 15 nm (Fig. 12(*a*)), 70 nm (Fig. 12(*b*)), 250 nm (Fig. 12(*c*)), and 690 nm (Fig. 12(*d*)). In addition, the case without overcoat is shown in Fig. 12(*e*). For the dimple contacting an uncoated gimbal, the largest maximum principal tensile stress is 155 MPa (Fig. 12(*e*)). This value is close to the largest maximum

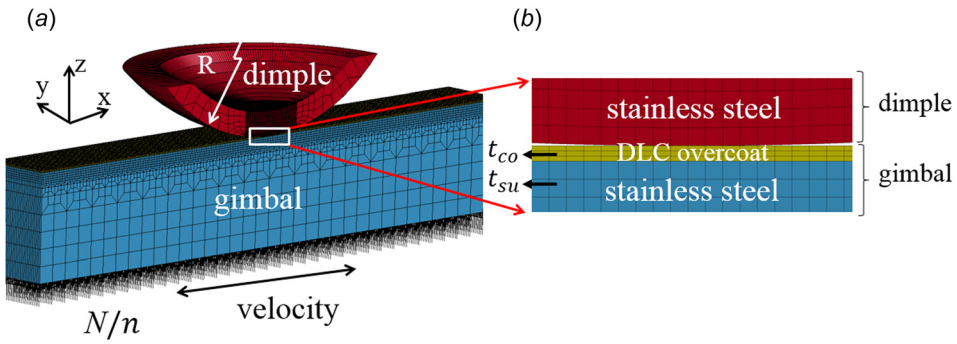

Fig. 10 Finite element model for contact between dimple and gimbal

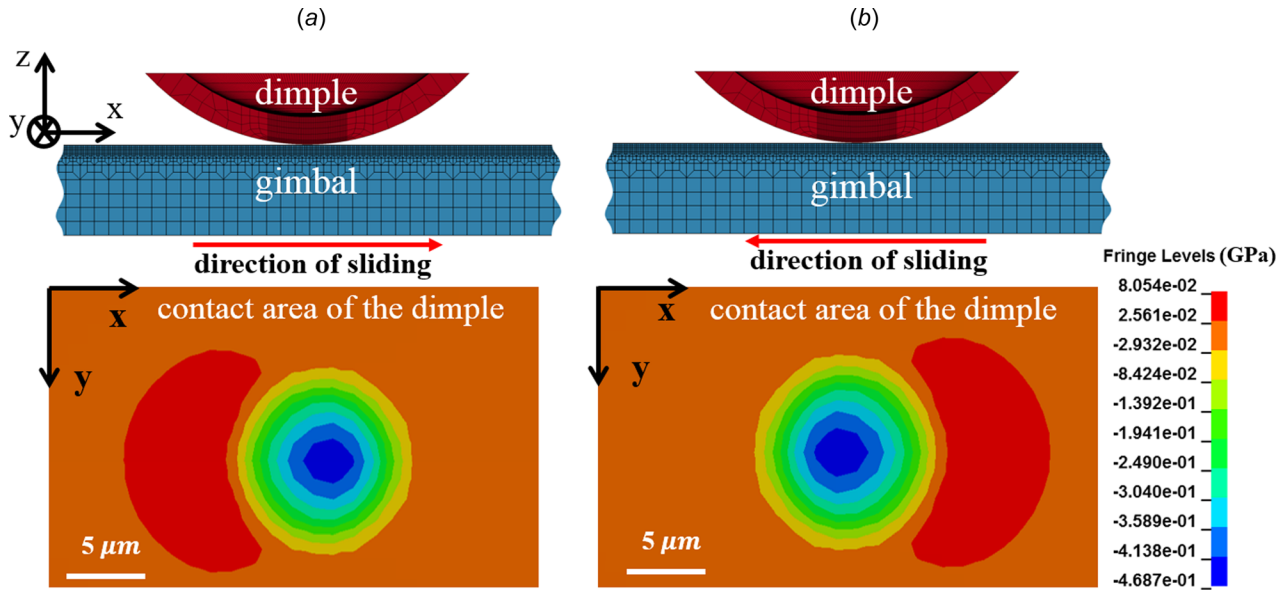

Fig. 11 Distribution of the maximum principal stress around the contact area of the dimple when the gimbal coated with 690 nm DLC slides in (*a*) positive *x* direction and (*b*) negative *x* direction

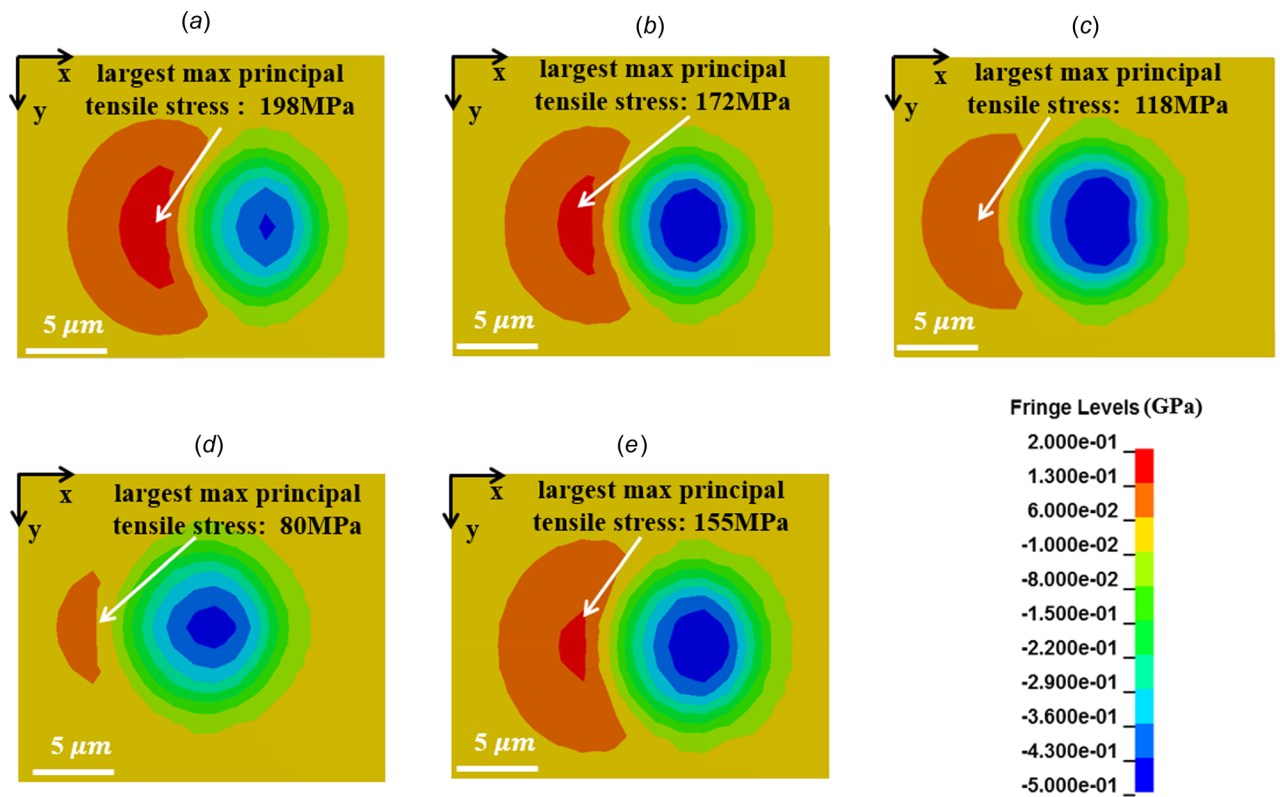

Fig. 12 Distribution of the maximum principal stress around the contact area of the dimple contacting (*a*) 15 nm DLC-coated gimbal, (*b*) 70 nm DLC-coated gimbal, (*c*) 250 nm DLC-coated gimbal, (*d*) 690 nm DLC-coated gimbal, and (*e*) uncoated gimbal when gimbals move in the positive *x* direction

principal tensile stress of 172 MPa for the case of 70 nm DLC overcoat (Fig. 12(*b*)). Cracks are observed in both contact areas (Figs. 7(*b*) and 7(*e*)). The dimple contacting a gimbal coated with 250 nm DLC shows the largest maximum principal tensile stress of 118 MPa (Fig. 12(*c*)), which is smaller than in the previous two cases. Therefore, crack formation should be less severe than in the other two cases. We observe from Fig. 7(*c*) that this is indeed the case, i.e., cracks are not as large as in the previous two cases (Figs. 7(*b*) and 7(*e*)). The largest maximum principal tensile stress of 80 MPa is observed for the case of 690 nm DLC (Fig. 12(*d*)). In this case, cracks are absent from the contact surface (Fig. 7(*d*)). For the dimple contacting a gimbal with 15 nm DLC, the largest maximum principal tensile stress is 198 MPa (Fig. 12(*a*)). This stress caused delamination as shown in Fig. 7(*a*). Comparing the SEM images in Fig. 7 and the largest maximum principal tensile stress in Fig. 12, we observe that cracks are larger for dimples

with higher maximum principal tensile stress. This suggests that the maximum principal tensile stress is indeed a good indicator in explaining the wear results. The different amount of wear and the different length of cracks observed appear to be related to the different level of maximum principal tensile stress in the dimples. The effect of a different value of the maximum principal tensile stress is magnified after a large number of fretting wear cycles, leading to a significant difference in the length of the cracks on the dimple.

Figure 12 shows furthermore that the largest maximum principal tensile stress occurs at the edge of the contact zone. This suggests that the microcracks observed in the fretting wear tests initiated at the edge of the contact zone. This has been observed in Refs. [34,35]. As can be inferred from Figs. 7(*b*) and 7(*c*), several cracks can form and propagate in the region near the contact zone. During the propagation of these cracks, merging or "coalescing" of individual cracks may occur, which eventually leads to large-scale delamination as shown in Fig. 7(*a*). The effect of merging of fatigue cracks was observed and discussed in an experimental study of fretting fatigue by Dubourg [36].

From the numerical results, we can also obtain the von Mises stress around the contact area of the dimple. As shown in Fig. 13, the dimple contacting a gimbal coated with 15 nm DLC (Fig. 13(*a*)) shows the highest von Mises stress, and the dimple contacting a gimbal coated with 690 nm DLC (Fig. 13(*d*)) shows the lowest von Mises stress. Dimples in the other three cases (Figs. 13(*b*), 13(*c*), and 13(*e*)) show intermediate levels of the von Mises stress. This trend is in accordance with the trend observed for the values of the maximum principal tensile stress.

Figure 14 shows the von Mises stress around the contact area for the case that 690 nm DLC-coated gimbal moves in the positive x direction (Fig. 14(*a*)) and the negative x direction (Fig. 14(*b*)). We observe that the location where the maximum von Mises stress occurs is at the center of the contact area for both cases. This location does not change with the direction of motion of the gimbal. In addition, we observe that the von Mises stress at the edge of the contact zone is independent of the direction of motion. Comparing the simulation results of the von Mises stress (Fig. 14) with the maximum principal stress results (Fig. 11), we find that the maximum principal stress is more suitable for studying crack formation in fretting wear because it changes with each cycle, causing fatigue cracks due to the alternating stress. For other wear situations, however, it is conceivable that the von Mises stress may be an equally good or better wear predictor, especially for ductile materials undergoing plastic deformation [37–39].

4.3 Stress Distribution in the Gimbal. Figure 15 shows the distribution of the maximum principal stress around the contact area of a gimbal coated with 690 nm DLC, sliding in the positive (Fig. 15(*a*)) and negative x direction (Fig. 15(*b*)). Similar to the dimple, the location where the largest maximum principal tensile stress occurs changes if the direction of motion of the gimbal reverses. Cyclic stresses are applied to the edge of the contact zone as the gimbal moves back and forth. Hence, microcracks generated at the gimbal surface could be categorized as fretting fatigue cracks.

Figure 16 shows numerical results for the maximum principal stress around the contact area of a gimbal with a carbon overcoat thickness of 0, 15 nm, 70 nm, 250 nm, and 690 nm, respectively, moving in the positive x direction. We observe that the uncoated gimbal has a maximum principal tensile stress of 178 MPa (Fig. 16(*e*)). A large amount of wear debris and large cracks was produced on the wear scar (Fig. 8(*e*)). The gimbal coated with 15 nm DLC shows the largest maximum principal tensile stress of 729 MPa (Fig. 16(*a*)). However, wear and crack formation on this wear scar (Fig. 8(*a*)) are less pronounced than on the uncoated gimbals (Fig. 8(*e*)). This is related to the higher hardness of the 15 nm DLC overcoat. The largest maximum principal tensile stress for gimbals coated with 70 nm (Fig. 16(*b*)) and 250 nm DLC

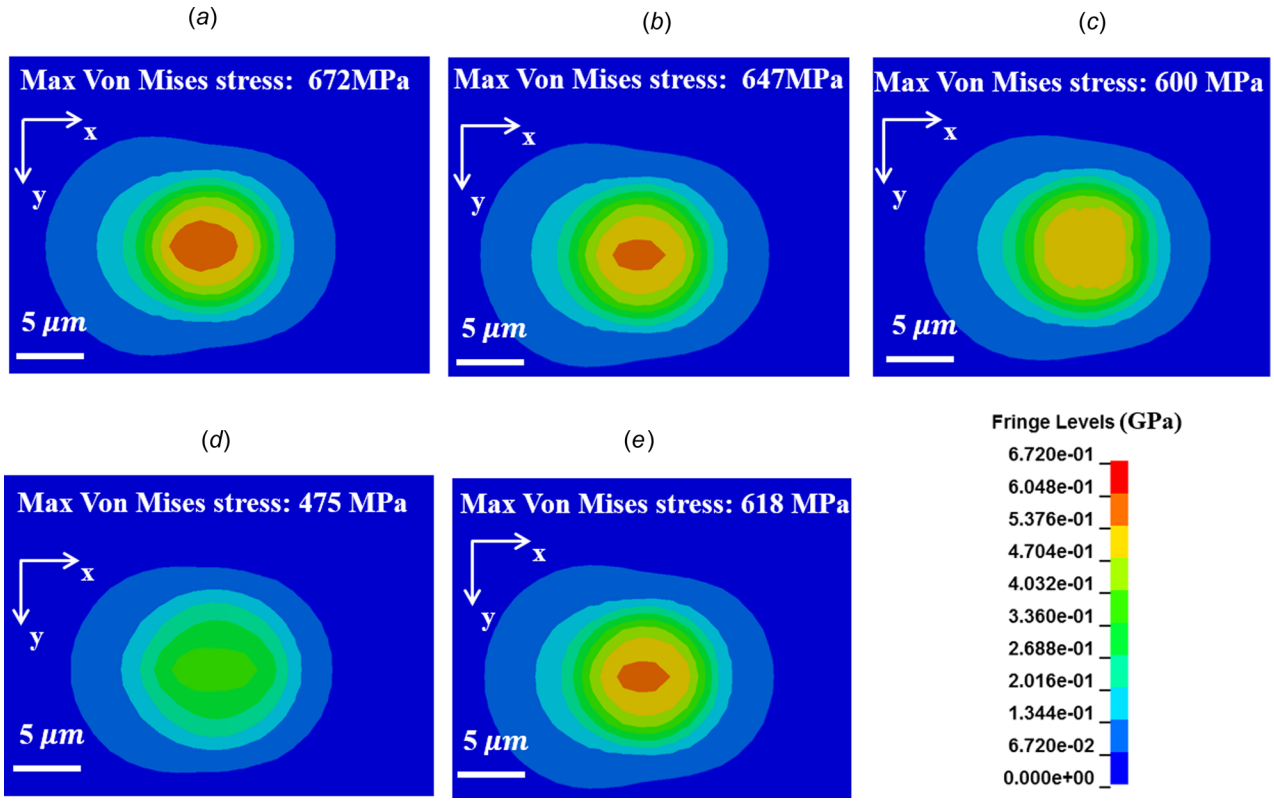

Fig. 13 Distribution of the von Mises stress around the contact area of the dimple contacting (*a*) 15 nm DLC-coated gimbal, (*b*) 70 nm DLC-coated gimbal, (*c*) 250 nm DLC-coated gimbal, (*d*) 690 nm DLC-coated gimbal, and (*e*) uncoated gimbal when gimbals move in the positive *x* direction

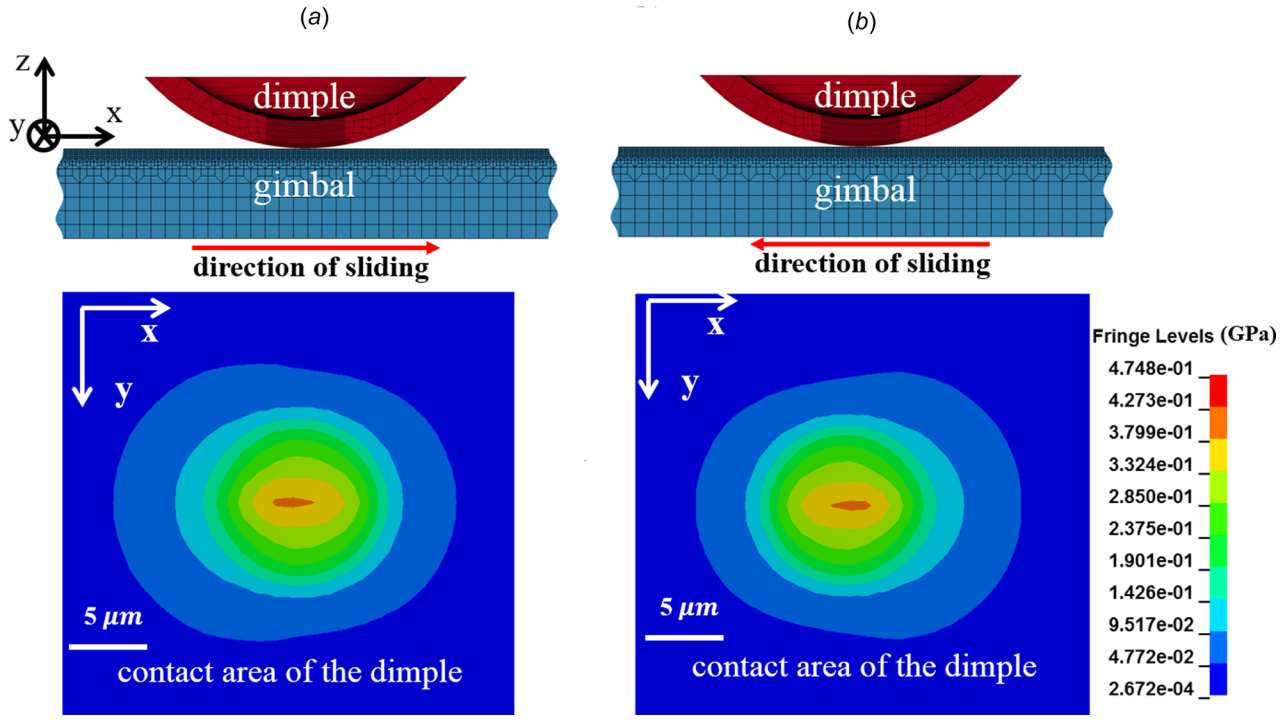

Fig. 14 Distribution of the von Mises stress around the contact area of the dimple when the gimbal coated with 690 nm DLC slides in (*a*) positive *x* direction and (*b*) negative *x* direction

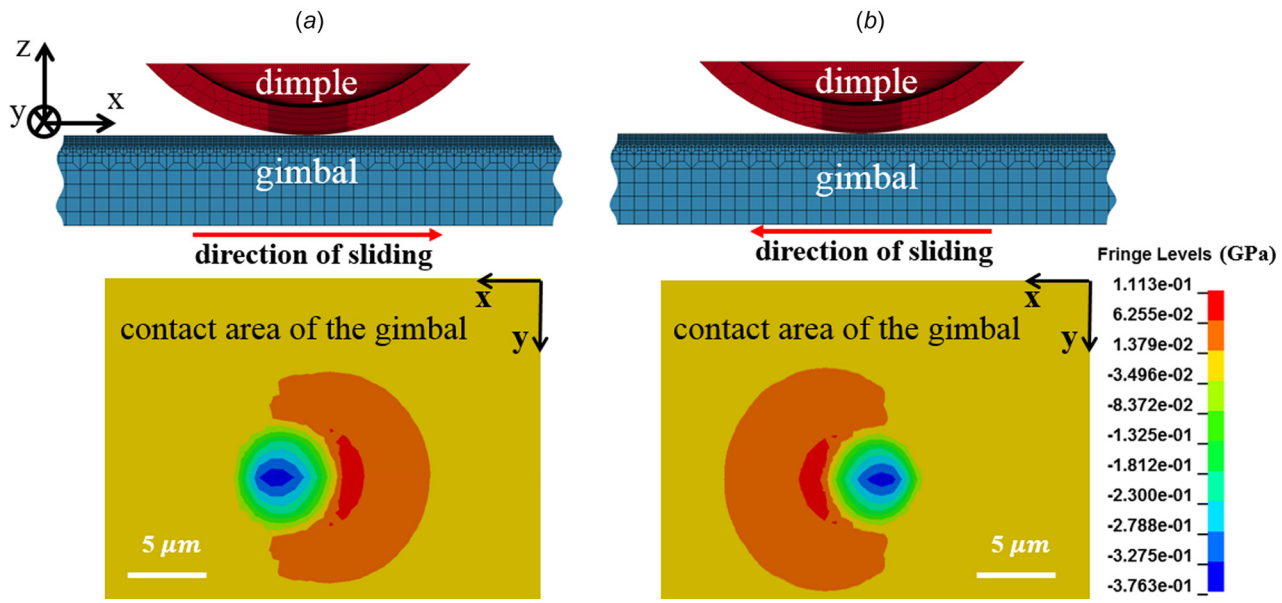

Fig. 15 Distribution of the maximum principal stress around the contact area of the gimbal when the gimbal coated with 690 nm DLC slides in (*a*) positive *x* direction and then in (*b*) negative *x* direction

(Fig. 16(*c*)) is 256 MPa and 278 MPa, respectively. These values are much smaller than the largest maximum principal tensile stress value for the gimbal coated with 15 nm DLC (Fig. 16(*a*)). However, a large amount of wear particles and long cracks was observed for these cases (Figs. 8(*b*) and 8(*c*)), most likely related to the lower hardness of the DLC overcoat. For a gimbal coated with 690 nm DLC, surface damage was small (Fig. 8(*d*)). This case is characterized by a low value of the largest maximum principal tensile stress of 111 MPa (Fig. 16(*d*)). Comparing the simulation results (Fig. 16) with the experimental results (Fig. 8), we can conclude that high maximum principal tensile stress in the gimbal does not seem to cause an increase in the amount of wear or an increase in the length of cracks formed. For gimbals with DLC overcoat, the amount of wear and the size of cracks generated during a fretting wear test are likely affected by the hardness of the DLC.

4.4 Effect of the Elastic Modulus of DLC Overcoat. Since the experimental results show that wear and cracks are predominantly generated on the dimple, numerical simulations were performed to investigate the effect of the elastic modulus of the DLC overcoat on the maximum principal stress in the dimple as a function of the DLC overcoat thickness (70 nm and 690 nm). For this calculation, we assumed a constant coefficient of friction of 0.28 between the dimple and the gimbal in both cases. The elastic modulus of the DLC overcoat was taken to vary from 70 GPa to 400 GPa. In Fig. 17, we plot the largest maximum principal tensile

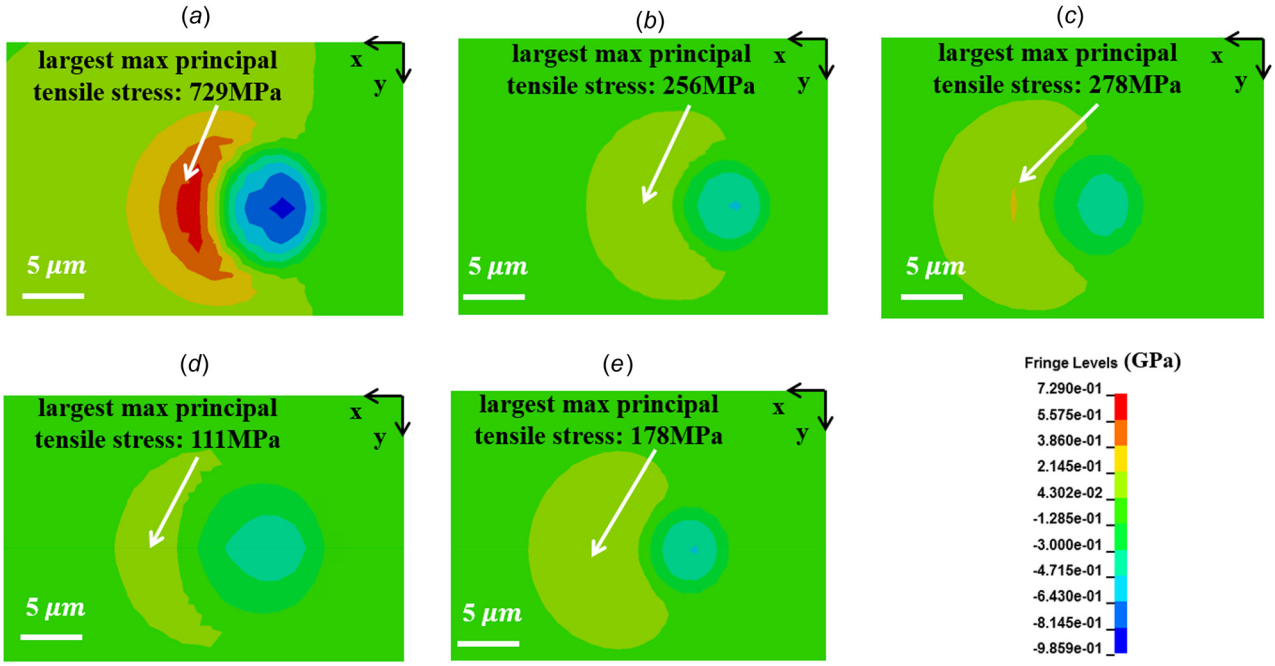

Fig. 16 Distribution of the maximum principal stress around the contact area of (*a*) 15 nm DLC-coated gimbal, (*b*) 70 nm DLC-coated gimbal, (*c*) 250 nm DLC-coated gimbal, (*d*) 690 nm DLC-coated gimbal, and (*e*) uncoated gimbal sliding in the positive *x* direction against dimples

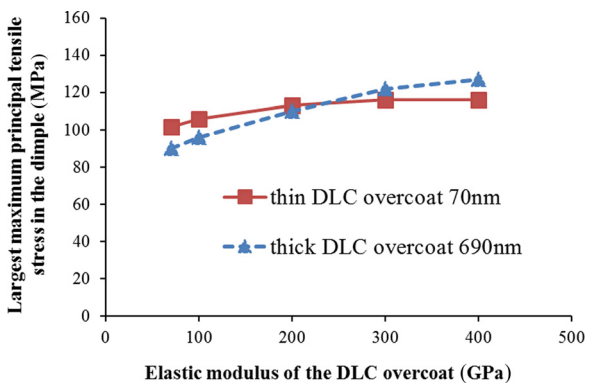

Fig. 17 The largest maximum principal tensile stress in the dimple contacting a gimbal coated with 70 nm and 690 nm DLC of different elastic moduli, assuming the friction coefficient is constant

stress as a function of the elastic modulus of the DLC overcoat for a "thin" (70 nm) and a "thick" (690 nm) overcoat. The 690 nm DLC overcoat with a low elastic modulus of 70 GPa shows the smallest maximum principal tensile stress. This is attributed to the low elastic modulus, and, therefore, the low effective elastic modulus of the gimbal, leading to a larger contact area and a lower contact stress than in the other cases with higher elastic modulus. In addition, the largest maximum principal tensile stress in the dimple increases as the elastic modulus of the DLC overcoat increases. This suggests that for both 70 nm and 690 nm DLC overcoats on the gimbal, an increase in the elastic modulus of the DLC overcoat leads to a larger contact stress, which may cause a larger amount of wear and longer cracks on the dimple during fretting wear. We also observe from Fig. 17 that the increase of the largest maximum principal tensile stress in a dimple contacting a 690 nm DLC overcoat is greater than the increase of the largest maximum principal tensile stress in a dimple contacting a 70 nm DLC overcoat. This situation can be qualitatively explained by the Hertzian contact theory [21]. The maximum contact pressure p_0 for the contact between a sphere and a flat half-space is given by

$$p_0 = \frac{1}{\pi}\left(\frac{6NE_*^2}{R^2}\right)^{1/3} \tag{5}$$

Here, N is the applied normal force, R is the radius of the sphere, and E_* is the "combined-effective" elastic modulus of the dimple and the gimbal defined by

$$\frac{1}{E_*} = \frac{1-v_1^2}{E_1} + \frac{1-v_2^2}{E_2} \tag{6}$$

where E_1 and E_2 are the elastic moduli, and v_1 and v_2 are the Poisson's ratios of the sphere and the half-space, respectively. We assume that v_1 and v_2 are both equal to 0.3. For the contact between the dimple and the gimbal, E_1 is the elastic modulus of the dimple, and E_2 is the effective modulus of the gimbal coated with DLC. For both the 70 nm and the 690 nm DLC overcoats, the increased elastic modulus of the overcoat increases the effective modulus of the gimbal E_2 in Eq. (6) and thus E_* in Eqs. (5) and (6). Since the DLC overcoat of 690 nm thickness has a greater influence on the effective elastic modulus of the gimbal than the thinner 70 nm DLC overcoat, E_2 and E_* of the gimbal coated with 690 nm DLC increase more as the elastic modulus of the DLC overcoat increases. Therefore, the contact pressure and the largest maximum principal tensile stress for a dimple contacting a 690 nm DLC overcoat increase more than for a dimple contacting a 70 nm DLC overcoat.

The results also show that the rate of increase in the largest maximum principal tensile stress in the dimple decreases as the elastic modulus of the DLC overcoat increases. As shown in Fig. 17, the largest maximum principal tensile stress does not increase significantly for either the 70 nm or the 690 nm overcoat, if the elastic modulus of the DLC overcoat increases from 300 GPa to 400 GPa. This suggests that a further increase of the elastic modulus of the DLC overcoat does not lead to a larger amount of wear or longer cracks on the dimple.

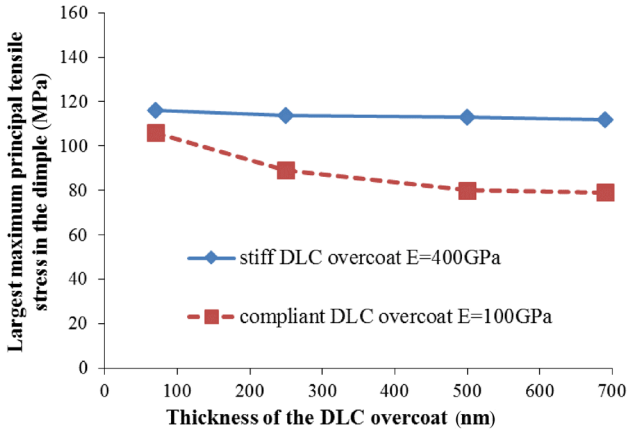

Fig. 18 The largest maximum principal tensile stress in the dimple contacting a gimbal coated with stiff and compliant DLC overcoat of different thickness, assuming the friction coefficient is constant

4.5 Effect of the Thickness of DLC Overcoat. In Fig. 18, we plot the largest maximum principal tensile stress as a function of the thickness of the DLC overcoat for a "compliant" (100 GPa) and a "stiff" (400 GPa) overcoat. For both cases, a constant coefficient of friction of 0.28 between the dimple and the gimbal was assumed. As seen in Fig. 18, the largest maximum principal tensile stress in the dimple contacting the DLC overcoat with elastic modulus of 400 GPa is almost constant. This can be explained by Eqs. (5) and (6). For the dimple contacting a DLC overcoat with an elastic modulus of 400 GPa, the increase in the thickness of the stiff DLC overcoat increases the effective elastic modulus of the gimbal E_2 in Eq. (6). However, the first term in Eq. (6) with the smaller elastic modulus E_1 of the dimple material dominates Eq. (6). Therefore, the influence of the thickness of the 400 GPa DLC overcoat on E_* in Eqs. (5) and (6) is small, and the maximum contact stress in Eq. (5) does not change significantly. For the gimbal coated with a DLC layer having an elastic modulus of 100 GPa, the effective elastic modulus of the gimbal E_2 decreases, although the thickness of the coating increases. This leads to a smaller E_* and a smaller contact pressure according to Eqs. (5) and (6). Consequently, the largest maximum principal tensile stress in the dimple decreases from 106 MPa to 80 MPa, while the thickness of the DLC overcoat increases from 70 nm to 690 nm. This suggests that less wear and shorter cracks occur if the thickness of the compliant DLC overcoat increases, assuming the friction coefficient is constant.

5 Conclusion

In this paper, both the experimental and numerical studies were performed to investigate the effect of a DLC overcoat on the tribological performance of the dimple/gimbal interface in hard disk drives. From the experimental results, we have found that: (1) Stainless steel dimples in contact with a 690 nm thick carbon-coated gimbal show the lowest friction coefficient and the smallest amount of wear debris compared to dimples in contact with gimbals having thinner carbon overcoats (15 nm, 70 nm, and 250 nm); (2) For stainless steel dimples contacting gimbals coated with DLC, wear particles at the dimple/gimbal interface are generated mostly on the dimple; and (3) DLC overcoats on the gimbal can improve the tribological performance of the gimbal, but may increase wear and cracks on the dimple.

From the simulation results, we observe that: (1) The maximum principal tensile stress is a good measure for analyzing fretting wear results. The amount of wear and the size of cracks observed experimentally are related to the maximum principal tensile stress in the dimple; (2) The dimple contacting a gimbal coated with a stiff DLC overcoat exhibits large maximum principal tensile stress, which leads to the generation of wear particles and large cracks on the dimple; (3) Stiff DLC overcoats cause large maximum principal tensile stress in the gimbal, but do not lead to an increase in wear and the size of cracks on the gimbal because of the high hardness of the DLC overcoats; and (4) With respect to the effect of thickness of the DLC overcoat, if the DLC overcoat is "stiffer" than the substrate, the thickness of the DLC overcoat does not have a significant influence on the level of stress in the dimple. On the other hand, if the DLC overcoat is more compliant than the substrate, an increase in the thickness of the DLC overcoat reduces the level of stress in the dimple.

To achieve the best tribological performance of the dimple/gimbal interface, the elastic modulus and the thickness of the carbon overcoat on the gimbal need to be optimized simultaneously. Based on the experimental and simulation results of this study, we conclude that a compliant and thick carbon overcoat on the gimbal is best for the tribological performance of the dimple/gimbal interface. A compliant and thick carbon overcoat causes low contact stress at the dimple/gimbal interface and can significantly reduce the generation of wear particles and the formation of cracks on both the dimple and the gimbal. To deposit a thick DLC overcoat with good tribological properties on the gimbal, it is crucial that the DLC layer has a uniform thickness and a uniform sp^3 bonding ratio. In addition, it is desirable that low residual stress is present in the DLC layer in order to prevent delamination [40].

The normal load between the sphere and the coated half-space in our study was kept constant at 20 mN, and the material deformation in our simulation was in the elastic range. In other industrial applications, the normal load can be much higher. This may lead to elastic–plastic deformation of the coating and the substrate [41]. The coating thickness investigated in our study was in the range from 15 nm to 690 nm, and the elastic modulus of the substrate was kept constant at 200 GPa. In other contact problems, the coating can be much thicker and the elastic modulus of the substrate can vary in the range of several hundred gigapascal. The different ranges of the coating thickness and the elastic modulus of the substrate lead to different substrate effects on the contact stresses. Therefore, it is difficult to predict a priori what will happen for different values of load, thickness, and elastic modulus of the overcoat. To find the optimized elastic modulus and overcoat thickness for other cases, finite element calculations may need to be performed for each particular situation.

Acknowledgment

The authors would like to thank Hanya-San, John Hogan, and Ross Cuyler of NHK Spring Corporation for their support of this research project. We also thank Young Woo Seo, Karcher Morris, and Benjamin Suen for their help with the experimental setup, and Tzong-Shii Pan and Lifan Chen of Western Digital Corporation for their help with the EELS measurements. The authors also thank Professor Izhak Etsion for helpful discussions and his insight in the mechanics of fretting wear.

References

[1] Vingsbo, O., and Söderberg, S., 1988, "On Fretting Maps," Wear, **126**(2), pp. 131–147.
[2] Raeymaekers, B., Helm, S., Brunner, R., Fanslau, E. B., and Talke, F. E., 2009, "Fretting Wear Between a Hollow Sphere and Flat Surface," ASME Paper No. IJTC2009-15208.
[3] Raeymaekers, B., Helm, S., Brunner, R., Fanslau, E. B., and Talke, F. E., 2010, "Investigation of Fretting Wear at the Dimple/Gimbal Interface in a Hard Disk Drive Suspension," Wear, **268**(11–12), pp. 1347–1353.
[4] Yoon, Y., Etsion, I., and Talke, F. E., 2011, "The Evolution of Fretting Wear in a Micro-Spherical Contact," Wear, **270**(9–10), pp. 567–575.
[5] Li, L., Fanslau, E. B., and Talke, F. E., 2011, "An Experimental Study of the Dimple/Gimbal Interface in a Hard Disk Drive," Microsyst. Technol., **17**(5–7), pp. 863–868.
[6] Li, L., Zheng, H., Fanslau, E. B., and Talke, F. E., 2011, "A Numerical Study of the Dimple Gimbal Interface in a Hard Disk Drive," Microsyst. Technol., **17**(5–7), pp. 869–873.

[7] Dearnley, P. A., 1999, "A Review of Metallic, Ceramic and Surface-Treated Metals Used for Bearing Surfaces in Human Joint Replacements," Proc. Inst. Mech. Eng., Part H, **213**(2), pp. 107–135.
[8] Vanhulsel, A., Velasco, F., Jacobs, R., Eersels, L., Havermans, D., Roberts, E. W., Sherrington, I., Anderson, M. J., and Gaillard, L., 2007, "DLC Solid Lubricant Coatings on Ball Bearings for Space Applications," Tribol. Int., **40**(7), pp. 1186–1194.
[9] Shi, B., Ajayi, O. O., Fenske, G., Erdemir, A., and Liang, H., 2003, "Tribological Performance of Some Alternative Bearing Materials for Artificial Joints," Wear, **255**(7–12), pp. 1015–1021.
[10] Fouvry, S., Kapsa, P., Zahouani, H., and Vincent, L., 1997, "Wear Analysis in Fretting of Hard Coatings Through a Dissipated Energy Concept," Wear, **203–204**(96), pp. 393–403.
[11] Liu, Y., Erdemir, A., and Meletis, E. I., 1996, "A Study of the Wear Mechanism of Diamond-Like Carbon Films," Surf. Coat. Technol., **82**(1–2), pp. 48–56.
[12] Kato, K., 2000, "Wear in Relation to Friction—A Review," Wear, **241**(2), pp. 151–157.
[13] Pharr, G. M., and Oliver, W. C., 1992, "Measurement of Thin Film Mechanical Properties Using Nanoindentation," Mrs Bull., **17**(7), pp. 28–33.
[14] Saha, R., and Nix, W. D., 2002, "Effects of the Substrate on the Determination of Thin Film Mechanical Properties by Nanoindentation," Acta Mater., **50**(1), pp. 23–38.
[15] Robertson, J., 1988, "Gap States in Amorphous Carbon," Philos. Mag. Lett., **57**(2), pp. 143–148.
[16] Xu, S., Flynn, D., Tay, B. K., Prawer, S., Nugent, K. W., Silva, S. R. P., Lifshitz, Y., and Milne, W. I., 1997, "Mechanical Properties and Raman Spectra of Tetrahedral Amorphous Carbon Films With High sp3 Fraction Deposited Using a Filtered Cathodic Arc," Philos. Mag. Part B, **76**(3), pp. 351–361.
[17] Xie, Y., and Williams, J. A., 1996, "The Prediction of Friction and Wear When a Soft Surface Slides Against a Harder Rough Surface," Wear, **196**(1–2), pp. 21–34.
[18] Savvides, N., and Bell, T. J., 1993, "Hardness and Elastic Modulus of Diamond and Diamond-Like Carbon Films," Thin Solid Films, **228**(1–2), pp. 289–292.
[19] Korsunsky, A. M., McGurk, M. R., Bull, S. J., and Page, T. F., 1998, "On the Hardness of Coated Systems," Surf. Coat. Technol., **99**(1–2), pp. 171–183.
[20] Szolwinski, M. P., and Farris, T. N., 1996, "Mechanics of Fretting Fatigue Crack Formation," Wear, **198**(1–2), pp. 93–107.
[21] Johnson, K. L., 1987, *Contact Mechanics*, Cambridge University Press, Cambridge, UK.
[22] Hamilton, G. M., 2006, "Explicit Equations for the Stresses Beneath a Sliding Spherical Contact," Proc. Inst. Mech. Eng., Part C, **197**(1983), pp. 53–59.
[23] Ling, F. F., Lai, M., and Lucca, D. A., 2002, *Fundamentals of Surface Mechanics With Applications*, Springer, New York.
[24] O'Sullivan, T. C., and King, R. B., 1988, "Sliding Contact Stress Field Due to a Spherical Indenter on a Layered Elastic Half-Space," ASME J. Tribol., **110**(2), pp. 235–240.
[25] Hallquist, J. O., 2006, *LS-DYNA Theoretical Manual*, Livermore Software Technology Corporation, Livermore, CA.
[26] Han, W., and Sofonea, M., 2002, *Quasistatic Contact Problems in Viscoelasticity and Viscoplasticity*, American Mathematical Society/International Press, Providence, RI.
[27] Waterhouse, R. B., 1992, "Fretting Fatigue," Int. Mater. Rev., **37**(2), pp. 77–97.
[28] Lamacq, V., and Dubourg, M. C., 1999, "Modeling of Initial Fatigue Crack Growth and Crack Branching Under Fretting Conditions," Fatigue Fract. Eng. Mater. Struct., **22**(6), pp. 535–542.
[29] Krupp, U., 2007, *Fatigue Crack Propagation in Metals and Alloys: Microstructural Aspects and Modelling Concepts*, Wiley, Weinheim, Germany.
[30] Sumi, Y., 2014, *Mathematical and Computational Analyses of Cracking Formation*, Springer, Tokyo.
[31] Okazaki, M., Yamada, H., and Nohmi, S., 1996, "Temperature Dependence of the Intrinsic Small Fatigue Crack Growth Behavior in Ni-Base Superalloys Based on Measurement of Crack Closure," Metall. Mater. Trans. A, **27A**(4), pp. 1021–1031.
[32] Paris, P. C., and Erdogan, F., 1960, "A Critical Analysis of Crack Propagation Laws," ASME J. Basic Eng., **85**(4), pp. 528–533.
[33] Haddad, M. H. E., Smith, K. N., and Topper, T. H., 1979, "Fatigue Crack Propagation of Short Cracks," ASME J. Eng. Mater. Technol., **101**(1), pp. 42–46.
[34] Hills, D. A., Nowell, D., and O'Connor, J. J., 1988, "On the Mechanics of Fretting Fatigue," Wear, **125**(1–2), pp. 129–146.
[35] Nishida, T., Kondoh, K., Xu, J.-Q., and Mutoh, Y., 2003, *Observations and Analysis of Relative Slip in Fretting Fatigue*, ASTM STP 1425, ASTM International, West Conshohocken, PA, pp. 33–43.
[36] Dubourg, M. C., 2003, *Local Fretting Regime Influences on Crack Initiation and Early Growth*, ASTM STP 1425, ASTM International, West Conshohocken, PA, pp. 206–219.
[37] Ashby, M. F., and Lim, S. C., 1990, "Wear-Mechanism Maps," Scr. Metall. Mater., **24**(5), pp. 805–810.
[38] Hutchings, I. M., 1992, *Tribology: Friction and Wear of Engineering Materials*, Butterworth-Heinemann, Ltd., Oxford, UK.
[39] Asaro, R. J., and Lubarda, V. A., 2006, *Mechanics of Solids and Materials*, Cambridge University Press, New York.
[40] Li, X., and Bhushan, B., 1996, "Micro/Nanomechanical and Tribological Characterization of Ultrathin Amorphous Carbon Coatings," J. Mater. Res., **14**(6), pp. 2328–2337.
[41] Holmberg, K., Laukkanen, A., Ronkainen, H., Wallin, K., Varjus, S., and Koskinen, J., 2006, "Tribological Contact Analysis of a Rigid Ball Sliding on a Hard Coated Surface—Part II: Material Deformations Influence of Coating Thickness and Young's Modulus," Surf. Coat. Technol., **200**(12–13), pp. 3810–3823.